Nature and Surface Interactions of Sulfur-Containing Deposits on V2O5-WO3/TiO2- Catalysts for SCR-DeNOx

Rammelt, T.; Kuc, A.; Böhm, J.; Heine, T.; Gläser, R.;

Originally published:

October 2019

Emission Control Science and Technology 5(2019), 297-306

DOI: https://doi.org/10.1007/s40825-019-00142-1

Emission Control Science and Technology

Nature and Surface Interactions of Sulfur-Containing Deposits on V2O5-WO3/TiO2-Catalysts for SCR-DeNOx

--Manuscript Draft--

Manuscript Number:	
Full Title:	Nature and Surface Interactions of Sulfur-Containing Deposits on V2O5-WO3/TiO2-Catalysts for SCR-DeNOx
Article Type:	Special Issue in honour of Professor Wolfgang Grünert
Funding Information:	
Abstract:	Sulfur-containing deposits form on a monolithic V2O5-WO3/TiO2 (VWT) catalyst during SCR-DeNOx with NH3 at 473 and 523 K and pressures up to 500 kPa in the presence of SO2 with sulfate contents of 1.7 to 13.0 wt.-%. Using TGA and DRIFTS, these deposits are determined to be mainly NH4HSO4 for SCR temperatures > 523 K. At lower temperatures, (NH4)2SO4 is formed. The thermal stability of NH4HSO4 supported on different transition metal oxides including V2O5, WO3, TiO2, MoO3 and Al2O3 varies with decomposition temperatures from 620 to 820 K. Using DFT calculations, it is show that the thermal stability of supported NH4HSO4 is mainly determined by hydrogen bonding of the HSO4- anions with the metal oxide surface. Increasing electronegativity of the metal atoms of the support oxide leads to weakening of the S-O bonds in the HSO4- anions and to lower decomposition temperatures of the supported NH4HSO4.
Corresponding Author:	Roger Gläser Universitat Leipzig Leipzig, Sachsen GERMANY
Order of Authors:	Roger Gläser
	Thomas Rammelt
	Agnieszka-Beata Kuc
	Jürgen Böhm
	Thomas Heine
Corresponding Author Secondary Information:	
Corresponding Author's Institution:	Universitat Leipzig
Corresponding Author's Secondary Institution:	
First Author:	Roger Gläser
First Author Secondary Information:	
Order of Authors Secondary Information:	
Author Comments:	

Nature and Surface Interactions of Sulfur-Containing Deposits on V_2O_5-WO_3/TiO_2-Catalysts for SCR-DeNO$_x$

Thomas Rammelt[a)], Agnieszka-Beata Kuc[b)], *Jürgen Böhm*[a)], *Thomas Heine*[b,c)], *Roger Gläser*[a)]

[a)] Institute of Chemical Technology, Universität Leipzig, Linnéstr. 3, 04103 Leipzig, Germany

[b)] Helmholtz-Zentrum Dresden-Rossendorf, Forschungsstelle Leipzig, Permoserstraße 15, 04318 Leipzig, Germany

[c)] Theoretical Chemistry, TU Dresden, Bergstraße 66c, 01062 Dresden, Germany

submitted to the *Special Issue in Honor of Prof. Dr. Wolfgang Grünert* in ***Emission Control Science and Technology***

corresponding author (roger.glaeser@uni-leipzig.de)

Abstract

Sulfur-containing deposits form on a monolithic V_2O_5-WO_3/TiO_2 (VWT) catalyst during SCR-DeNOx with NH_3 at 473 and 523 K and pressures up to 500 kPa in the presence of SO_2 with sulfate contents of 1.7 to 13.0 wt.-%. Using TGA and DRIFTS, these deposits are determined to be mainly NH_4HSO_4 for SCR temperatures > 523 K. At lower temperatures, $(NH_4)_2SO_4$ is formed. The thermal stability of NH_4HSO_4 supported on different transition metal oxides including V_2O_5, WO_3, TiO_2, MoO_3 and Al_2O_3 varies with decomposition temperatures from 620 to 820 K. Using DFT calculations, it is show that the thermal stability of supported NH_4HSO_4 is mainly determined by hydrogen bonding of the HSO_4^- anions with the metal oxide surface. Increasing electronegativity of the metal atoms of the support oxide leads to weakening of the S-O bonds in the HSO_4^- anions and to lower decomposition temperatures of the supported NH_4HSO_4.

Keywords

SCR, DeNOx, VWT, TGA, DFT, DRIFTS

1. Introduction

During the past decades, the selective catalytic reduction (SCR) of NO_X using NH_3 as a reducing agent has evolved into a state-of-the-art means for NO_X-emission control in heavy-duty diesel engine applications [1]. Using V_2O_5-WO_3/TiO_2-type (VWT) catalysts, high NO_X removal efficiency is achieved over a wide range of operating conditions [2]. More recently, the pre-turbine setup was introduced. In this setup, the catalytic converter is placed upstream of the turbine of an exhaust gas turbo charger. Thus, the catalytic converter can be operated at elevated pressures of up to 500 kPa [3–6]. The operation of the SCR catalyst at elevated pressure can enhance the efficiency of the NO_X removal process and can save catalytic material, thus increasing cost and space efficiency. However, side reactions such as the formation of SO_3 or the parasitic NH_3-oxidation can also be accelerated [7–9]. Especially for heavy-duty diesel engines, the oxidation of SO_2 to SO_3 becomes a major issue. Above all, the formation of sulfur-containing deposits such as $(NH_4)_2SO_4$ and NH_4HSO_4 can be formed from SO_3, H_2O and NH_3 present in the exhaust gas [10–15]. These sulfur-containing deposits can lead to blocking of the surface, the pores or even the channels of the catalyst, resulting in reduced NO_X removal efficiency and damage of the exhaust aftertreatment system [16,17].

The deactivation of VWT catalysts due to sulfate formation as well as the resistance of VWT catalysts against sulfur poisoning was broadly addressed [18–24]. Operation conditions leading to the formation of sulfur-containing deposits and operation windows avoiding the formation of these deposits have been investigated, too [18,21,25–32]. Nevertheless, Zhu et al. [33] have shown, using temperature-programmed decompositions experiments, that the NH_4HSO_4 loaded on different supports decomposes at different temperatures depending on the type of support material. Moreover, these authors have reported that TiO_2 as a support leads to a higher decomposition temperature than that of the unsupported NH_4HSO_4. These results were confirmed by Li et al. [34], who investigated the decomposition of NH_4HSO_4 on different activated carbons. In addition, both Zhu et al. [33] and Li et al. [34] found that NH_3 formed from decomposition of NH_4HSO_4 can react with NO from the gas phase to molecular nitrogen. The overall reaction rate of this reaction is directly linked to the decomposition temperature of NH_4HSO_4 as proven by temperature-programmed surface reaction experiments [33,34].

Furthermore, $(NH_4)_2SO_4$ can be converted with NO to NH_4HSO_4 [16]. Besides this conversion, $(NH_4)_2SO_4$ can decompose directly to NH_4HSO_4 under evolution of NH_3 [35,36]. Both the reaction of $(NH_4)_2SO_4$ with NO and its thermal decomposition may be the reason that in most studies only NH_4HSO_4 deposits on VWT catalysts are reported after operation under SCR conditions, even though formation of $(NH_4)_2SO_4$ is possible [25,37–40].

In addition to experimental data, also computational methods were applied to understand the behavior and interaction between different catalysts and catalyst poisons [41,42]. For instance, Du et al. [43] calculated the binding energies of different alkali metals to the active sites of V_2O_5-type catalysts. Thus, the poisoning strength of different alkali metals was explained with potassium being the most potent poison within the alkali metals. Broclawik et al. [44] calculated the binding interaction of water with surfaces of V_2O_5 and WO_3 and concluded that a mixed oxide of V_2O_5 and WO_3 will enhance the binding strength of water to the surface compared with the single oxides.

Despite the reports on sulfate formation, reactivity and thermal stability on a wide variety of support materials and catalysts, a systematic investigation on the influence of the tree main components of VWT catalysts, i.e., V_2O_5, WO_3, TiO_2, on the thermal stability of NH_4HSO_4 and the nature of its interaction with the surface of the oxides is not available. The aim of this study was, first, to study the nature of the sulfur-containing deposits formed on VWT catalysts during SCR-DeNOx in the presence of SO_2 including elevated pressures. Another goal was to investigate the thermal stability of NH_4HSO_4 supported on VWT catalysts and on its oxide components. For that purpose, thermogravimetric analysis and DRIFTS experiments were applied to understand the different interactions of NH_4HSO_4 with the components of a VWT catalyst, i.e., V_2O_5, WO_3, and TiO_2, respectively, in comparison with other transition metal oxides used as or catalysts and catalyst supports for SCR-$DeNO_x$. To provide further insight into the nature of the interaction of NH_4HSO_4 with different metal oxides, experimental spectroscopic data were compared to those calculated by the DFT method.

2. Experimental Section

2.1 Deposition of NH_4HSO_4

NH_4HSO_4 (98.5 wt.-%, Roth) was deposited by impregnation on a commercial monolithic VWT catalyst (as used in a previous study [7]), V_2O_5 (99.8%, Roth), WO_3 (99%, Aldrich), TiO_2 (HombiKat UV 100, Aldrich; anatas phase), MoO_3 (99.98%, Roth), Al_2O_3 (99%, Roth), and on a physical mixture of V_2O_5, WO_3, and TiO_2 (labeled as VWT-mixture, obtained by mixing and grinding of V_2O_5 (2 wt.-%), WO_3 (10 wt.-%) and TiO_2 (88 wt.-%)). To 1 g of material to be impregnated 10 mL of a 2.5 mg mL^{-1} (0.217 mol L^{-1}) solution of NH_4HSO_4 (98.5%, Roth) in deionized water was added dropwise under mixing at room temperature followed by drying in ambient air at 363 K over night [33].

2.2 Gas phase poisoning and catalytic experiments

Gas phase poisoning and catalytic experiments were conducted in a laboratory synthetic exhaust gas test bench as described elsewhere [7]. For all experiments, the commercial monolithic VWT catalyst (300 cpsi, 10 x 10 channels, 10 cm length) was used. For poisoning experiments, SO_2 was added to the feed gas and the overall time-on-stream was 14 h. Catalytic experiments were conducted consecutively at 473 and 523 K at stationary state (30 min on-stream). Sample codes and conditions for gas phase poisoning and catalytic experiments are given in Table 1. For the sample PT150, 10 channels were removed from the catalytic monolith for characterization. The catalyst with the remaining 9x10 channels was then used for the catalytic experiment.

Table 1: Sample code and reaction conditions of gas phase poisoning (PT) and for catalytic experiments (gas hourly space velocity GHSV, reaction temperature T, reaction pressure p and concentration c of the feed gas components NO, NH_3, O_2, H_2O and SO_2).

sample code	GHSV / h^{-1}	T / K	p / kPa	c(NO) / ppm	c(NH_3) / ppm	c(O_2) / vol.-%	c(H_2O) / vol.-%	c(SO_2) / ppm
PT1	60,000	523	100	500	500	8	5	250
PT5	60,000	523	500	500	500	8	5	250
PT150	60,000	423	100	500	500	8	5	250
catalytic experiment	60,000	473, 523	100	1000	1000	8	5	0

2.3 Characterization

All samples generated by gas phase poisoning were analyzed for sulfur content using optical emission spectrometry with inductively coupled plasma (ICP-OES, Optima 8000, PerkinElmer). Before characterization, the catalyst monoliths were cut into three

pieces of equal length (for labelling, catalyst front: –E, middle: –M, exit: –X), grinded into powder and dissolved (30 mg sample dissolved in 4 mL aqueous HF, HNO_3 and HCl solution in a microwave oven). The sulfate content (in wt.-%) was calculated from the sulfur content assuming that sulfur is present as sulfate only. The sulfate content of the commercial VWT catalyst was calculated as an average of the sulfate content of the three catalyst pieces.

2.4 Diffuse reflectance infrared spectroscopy (DRIFTS)

DRIFTS experiments were carried out using a Bruker Vector 22 fitted with an in-situ diffuse reflectance cell (Specac) and ZnSe as the IR-window. All spectra were collected at a resolution of 4 cm^{-1} by accumulation of 100 scans. For each experiment, the sample was mixed with KBr (Uvasol, Merk) in a mass ratio of 5:95, finely grinded, placed into the cell, and dried for 12 h at 423 K under N_2-flow (200 mL min^{-1}). The spectrum of pure KBr was used as the background.

2.5 Thermogravimetric analysis

Thermogravimetric analysis (TGA) was conducted in an STA409 instrument from Netzsch by heating 25 – 50 mg sample in a stream of N_2 (70 cm^3 min^{-1}) to 873 K with 10 K min^{-1}. During TGA the evolving SO_2 was continuously analyzed by mass spectrometry (QMG 421, Pfeiffer & Balzer) at m/z = 64.

2.6 Density Functional Theory studies

All density functional theory (DFT) calculations were performed with the ADF code using hybrid B3LYP functional [45–47]. The different metal oxides (V_2O_5, TiO_2, MoO_3) were treated with TZP basis set (for WO_3 ZORA-TZP was used). All geometries were fully optimized. As starting geometries, clusters containing two metal atoms, which were in agreement with the literature, were generated from the respective bulk systems [43,44,48]. Oxygen dangling bonds were saturated with hydrogen to compensate the charge. $(NH_4)_3(HSO_4)_2^+$, based on the known crystal structure, was used as the staring geometry representing the NH_4HSO_4 as the best compromise between calculation time and accuracy. This also prevents the decomposition of NH_4HSO_4 to NH_3 and H_2SO_4. Calculations were performed on the bonding states, electronegativities, and the Bader critical point analysis [49]. Based on optimized structures, the vibrational spectra were calculated using ADF.

3. Results and Discussion

3.1 Gas phase poisoning and catalytic activity

To investigate the poisoning effect of SO_2 from the gas phase, a commercial VWT catalyst was exposed to a synthetic exhaust gas mixture containing SO_2. As shown in Figure 1, the VWT catalyst after gas-phase poisoning reveals an increased sulfate content compared to the fresh catalyst. The sulfate content found in the fresh VWT catalyst results from the manufacturing process. Comparing the gas phase poisoned samples, the sulfate formation is mainly governed by the temperature rather than the pressure during poisoning. Thus, the highest sulfate content of 13.0 wt.-% was found for PT150 poisoned at 423 K, whereas PT1 and PT5, poisoned at 52223 K, exhibit a much lower sulfate content of 2.4 wt.-% and 1.7 wt.-%, respectively. Higher pressure does not result in a higher sulfate content of the catalyst as can be seen from the lower sulfate contents of sample PT5 than of sample PT1. A higher sulfate content could be expected due to the shift in thermodynamic equilibrium towards solid sulfate formation as well as due to the increased residence time of the gas mixture on the catalyst at higher pressure (at constant GHSV). Note, however, that the sulfate formation took place not only on the catalyst, but also in other parts of the catalytic apparatus. This effect was more pronounced at elevated pressure, leading to more sulfate deposition upstream rather than on the catalyst for PT5 with respect to PT1.

Note also, that the NO_X-conversion in the catalytic experiments is lower for higher sulfate content deposited on the catalyst (Figure 1). This is in good agreement with the literature and can be explained by blocking of pores and catalytically active sites due to sulfur-containing deposits [20,50].

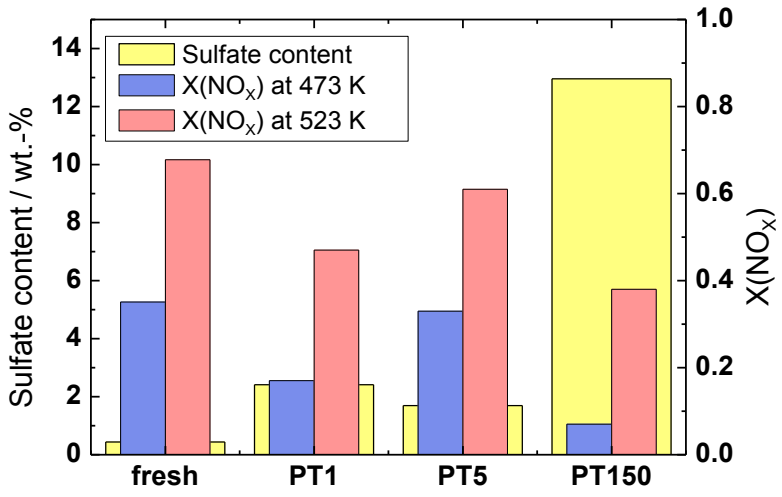

Fig. 1: Sulfate content and NO_X-conversion for fresh and gas phase poisoned commercial VWT catalyst samples (poisoning and reaction conditions as in Table 1).

3.2 Diffuse Reflectance Infrared Spectroscopy

DRIFTS spectra were recorded for the VWT catalysts after gas phase poisoning to identify the nature of the sulfur-containing deposits. In Figure 2, the spectra of NH_4HSO_4 and the VWT catalyst PT150-E with the highest sulfur content (cf. Fig. 1) are shown. Intense bands between 3500 and 2250 cm^{-1} and at around 1400 cm^{-1} indicate the presence of NH_4^+ species on the catalyst surface. Bands at 1220, 1132, 1058, 1042 and 974 cm^{-1} can be attributed to SO_4^{2-} and HSO_4^- species [18,28,29].

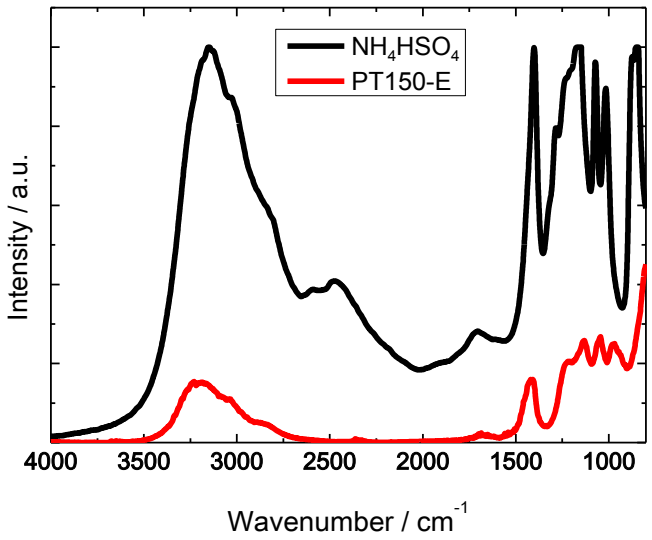

Fig. 2: DRIFTS spectra of NH_4HSO_4 and of the VWT catalyst PT150-E after catalytic experiment at 523 K.

Therefore, the detected deposits on the surface of the VWT catalyst after gas phase poisoning can be assigned to NH_4HSO_4. Similar bands are also observed for the catalysts after gas-phase poisoning with SO_2.at 523 K, i.e., PT1-E and PT5-E (not shown). However, as shown in Figure 3 (a), the spectra of the catalyst PT150-E before and after the catalytic experiment differ. Since also the spectra of NH_4HSO_4 and $(NH_4)_2SO_4$ differ (Figure 3 (b), in agreement with literature [51]), they can be used to identify the different sulfates. For PT150-E before the catalytic experiment, no characteristic bands for NH_4HSO_4 are observed (Figure 3 (a)). Accordingly, mainly

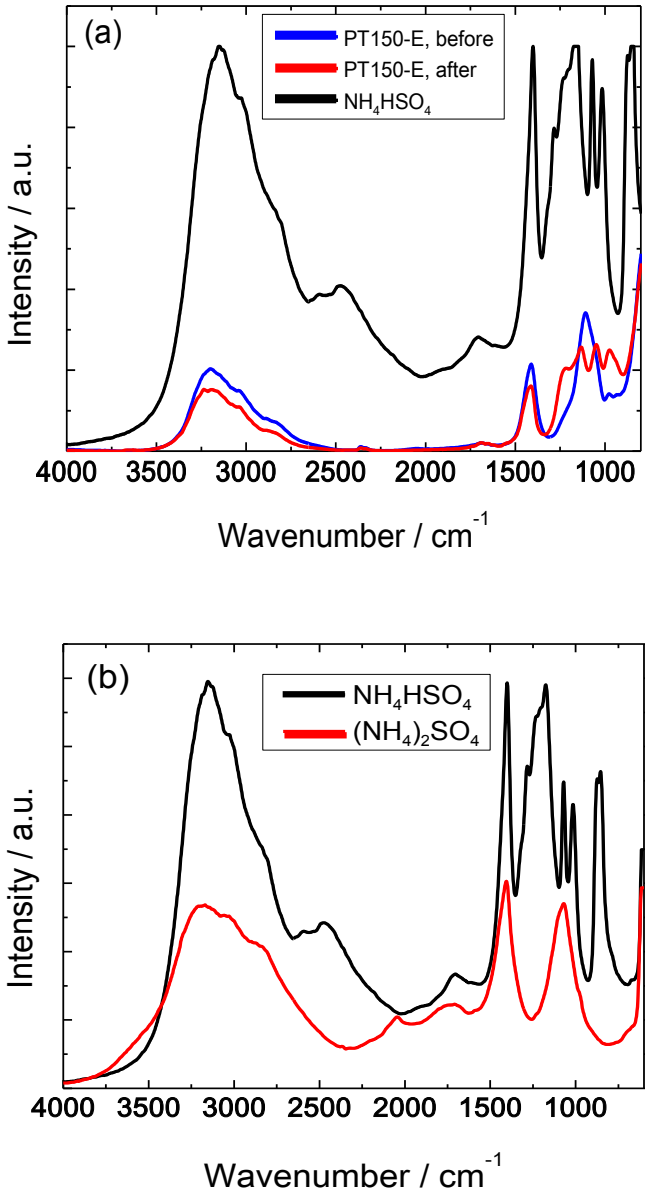

Fig. 3: DRIFTS spectra of PT150-E before and after the catalytic experiment at 423 K as well as NH_4HSO_4 (a) and of NH_4HSO_4 and $(NH_4)_2SO_4$) (b).

$(NH_4)_2SO_4$ was deposited during gas phase poisoning. Consequently, the (initially formed) deposits must have been changed during the catalytic experiments, even though they were carried out at a maximum temperature of 523 K, i.e., clearly below the decomposition temperature of $(NH_4)_2SO_4$ [35]. This can be explained by the reaction of $(NH_4)_2SO_4$ with NO under SCR reaction conditions at temperatures below 523 K as reported in several earlier studies [28–30,33]. Therefore, NH_4HSO_4 was used as a model substance for sulfur-containing deposits in all further experiments in this study.

In the DRIFTS spectra of V_2O_5, WO_3 and TiO_2 impregnated with NH_4HSO_4 (Figure 4) the band assigned to NH_4^+ at around 1400 cm^{-1} is observed. Also, bands around 1000 cm^{-1}, which can be assigned to HSO_4^+, are detected, although at different intensity and at different wavenumbers. This suggests that the interaction between NH_4HSO_4 and the surface is different for the three oxides. A further interpretation or assignment of the observed bands is, however, not possible due to the complexity of the spectra. Nevertheless, the DRIFTS experiments unambiguously show that NH_4HSO_4 is present on all three metal oxides and that they interact with the deposited NH_4HSO_4 in different ways.

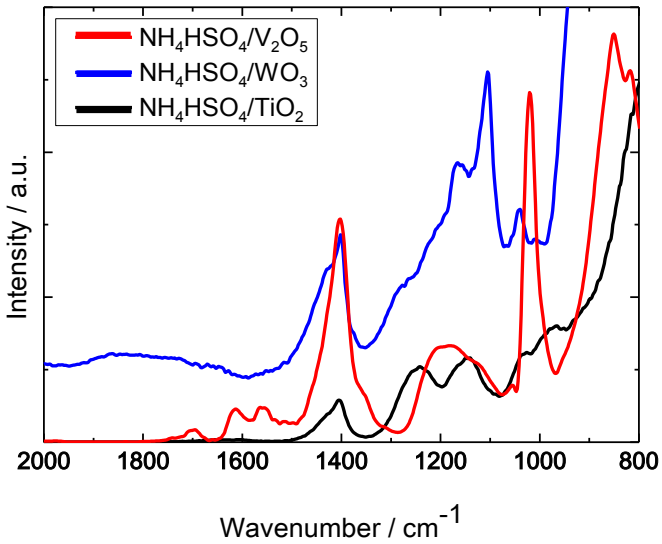

Fig. 4: DRIFTS spectra of NH_4HSO_4 on V_2O_5, WO_3 and TiO_2.

3.3 Thermogravimetric Analysis

In order to further understand the interaction of the deposited sulfate species with oxide surfaces, TGA experiments were carried out for gas phase poisoned or NH_4HSO_4-

impregnated samples. In Figure 5, the SO_2 evolution during TGA for the gas phase poisoned VWT catalysts PT1-E and PT5-E as well as for an NH_4HSO_4-impregnated VWT catalyst are shown. For all three catalysts, the maximum SO_2 evolution is observed at 695 K. This again confirms that NH_4HSO_4 is a suitable model substance for sulfur-containing deposits formed in the presence of SO_2 under SCR reaction conditions. In addition, the signal intensities at maximum SO_2 evolution are comparable for the three catalysts, thus indicating comparable amounts of deposited NH_4HSO_4. However, due to chemical reactions between SO_2 and the metal oxides forming surface sulfates, the absolute intensities of the SO_2 evolution signals will not be discussed here [52,53].

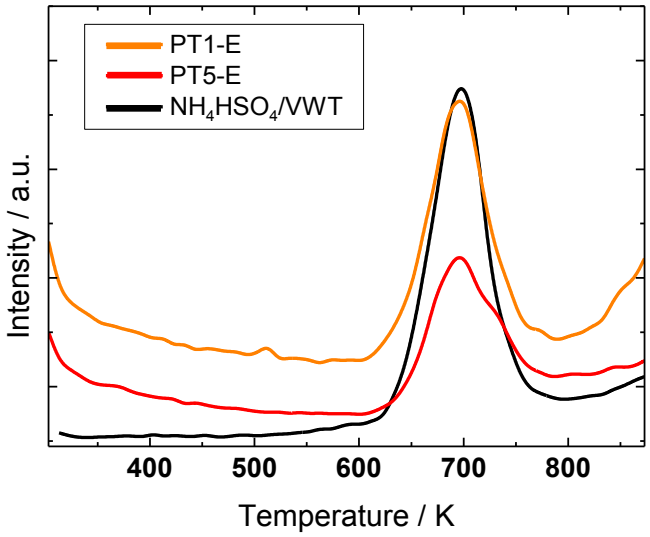

Fig. 5: Intensity of the MS-signal for m/z = 64 as a measure of SO_2-evolution during TGA of gas phase poisoned (PT1-E, PT5-E) and NH_4HSO_4-impregnated samples (NH_4HSO_4/VWT).

The thermal decomposition of NH_4HSO_4 when loaded on different metal oxides and on a VWT catalyst occur at distinctly different temperature (Figure 6). The decomposition of NH_4HSO_4 on V_2O_5 progresses in different steps, as already reported before [33]. According to this literature report, the decomposition temperature of NH_4HSO_4 supported on V_2O_5 and TiO_2 is higher than for the pure, unsupported salt as also observed here (NH_4HSO_4 decomposes completely with a maximum of differential weight loss during TGA at 473 K).

To get a deeper insight into the role of the different metal oxides included in a VWT catalyst, a mixture of WO_3, V_2O_5 and TiO_2 in comparable weight fractions as found on VWT catalysts was prepared and loaded with NH_4HSO_4. The decomposition of

NH_4HSO_4 on this mixture occurs in a similar temperature range as would be expected from the calculated weighted average of the single components, although not as a direct superposition of the contributions of the three oxides (Figure 7). However, this temperature range is significantly higher (maximum at 773 K) than that for the commercial VWT catalysts loaded with NH_4HSO_4 or the gas phase poisoned samples (695 K, cf. Fig. 5). A potential explanation is that the destabilizing effect of WO_3 on NH_4HSO_4 is incorrectly represented in the oxide mixture.

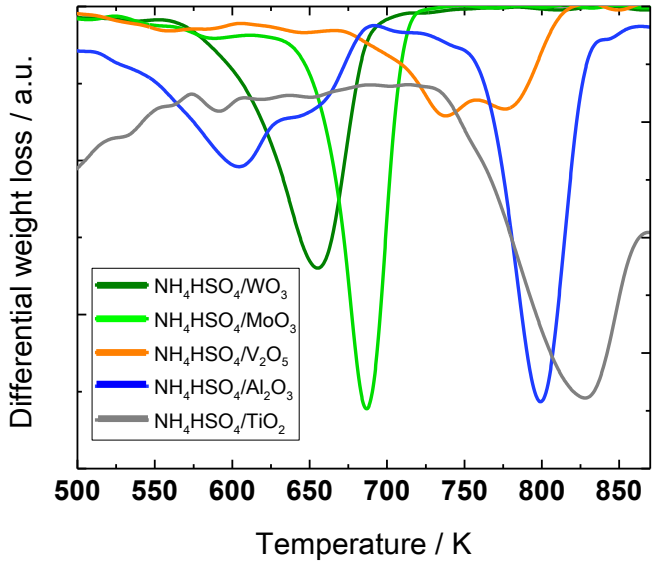

Fig. 6: Differential weight loss as a function of temperature during TGA of NH_4HSO_4 on different metal oxides.

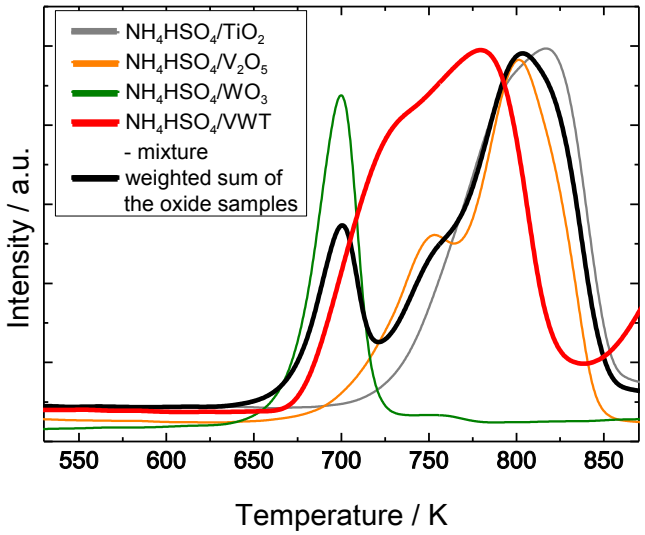

Fig. 7: Intensity of the MS-signal for m/z = 64 as a measure of SO_2-evolution during TGA on NH_4HSO_4 loaded on the VWT-mixture in comparison to the weighted sum (based on mass fraction of V_2O_5, WO_3 and TiO_2 in commercial VWT) of the metal oxides.

Figure 8 shows exemplary results of the TGA experiments for the gas phase poisoned catalyst PT150-E before and after the catalytic experiment. The main difference between TGA profiles of the two catalysts is the weight loss below 573 K. During the TGA experiment, no SO_2 evolution was detected for temperatures below 573 K on both samples. The weight loss is, therefore, assigned to the thermal decomposition of $(NH_4)_2SO_4$ to NH_4HSO_4 accompanied by NH_3-evolution, which is in a good agreement results from the DRIFTS experiments above (cf. section 3.2.) and with the literature [35].

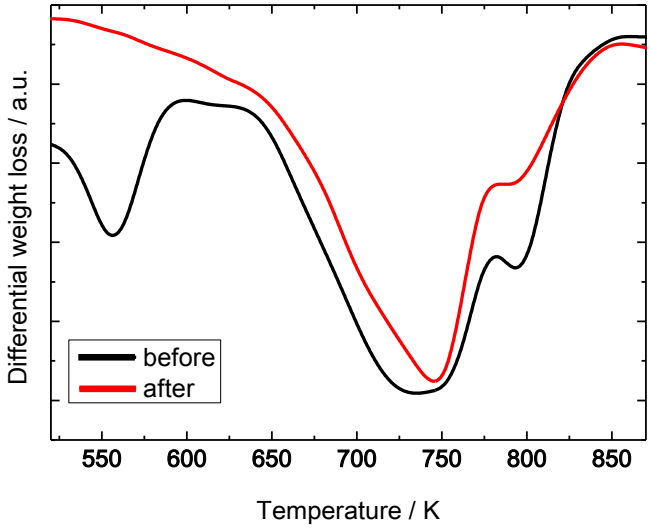

Fig. 8: Differential weight loss during TGA of the gas phase poisoned sample PT150-E before and after the catalytic experiment.

3.4 Calculations via Density Functional Theory

Based on the starting geometries from crystal structures, the most stable geometries for the systems $(NH_4)_3(HSO_4)_2^+$, NH_4HSO_4/WO_3, NH_4HSO_4/V_2O_5 and NH_4HSO_4/TiO_2 were calculated using the ADF software package [45–47]. In addition, topological analyses of the electron densities (Bader analyses) were performed for all investigated models. The resulting geometries and bonding maps resulting from Bader analysis are shown in Figure 9. It can be stated that the NH_4HSO_4 is mainly stabilized by hydrogen bonds, whereby the bonding interaction between the two HSO_4^- over one H-atom is crucial for the overall stability (Figure 9(a)), since the calculation of the most stable geometry of NH_4HSO_4 starting from only one NH_4^+ and one HSO_4^- results in the formation of NH_3 and H_2SO_4. This was not the case for NH_4HSO_4 placed near a metal oxide, which could be explained by the stabilization of either the NH_4^+ or the HSO_4^- by

hydrogen bonds formed with the OH-groups of the oxides, as shown in Figures 9 (b) - (d). However, the comparison of the geometries and bonding interactions of the NH_4HSO_4/metal-oxide systems clearly indicate significant differences in the interactions between the HSO_4^- and the surrounding species. Assuming stabilizing effects on the HSO_4^- of these bonding interactions, one can estimate qualitatively the thermal stability of the NH_4HSO_4 on different metal oxides according to the degree of interaction of the HSO_4^- with the surrounding species. Thus giving an increase in thermal stability of NH_4HSO_4 depending on the metal oxide in the order of $WO_3 < V_2O_5 < TiO_2$. However, it is not possible to estimate the thermal stability of pure NH_4HSO_4 compared to the NH_4HSO_4/metal-oxide systems, since the stabilizing effect of the interaction between two HSO_4^--ions is not accounted for in the NH_4HSO_4/metal-oxide systems.

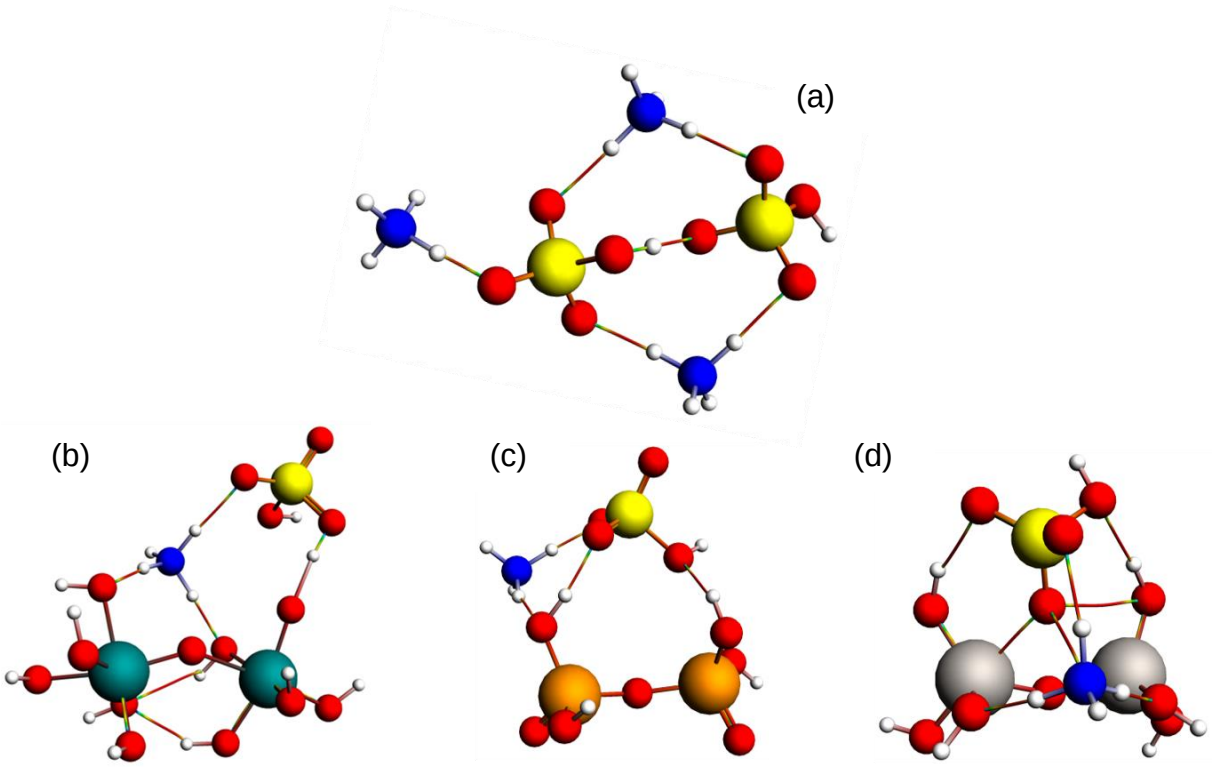

Fig. 9: Final geometries and bonding maps for (a) NH_4HSO_4, (b) NH_4HSO_4/WO_3, (c) NH_4HSO_4/V_2O_5 and (d) NH_4HSO_4/TiO_2 (H: white, N: blue, O: red, S: yellow, Ti: grey, V: orange, W: green).

Besides the hydrogen bond interactions between the NH_4HSO_4 and the metal oxides, for the TiO_2 based system, some additional interactions can be identified. As can be seen from Figure 9(d), there are direct interactions between one O-atom of the HSO_4^- and one Ti-atom, one O-atom from a Ti-OH-group and the N-atom of the NH_4^+, respectively. Especially the interactions between the O-atom from the HSO_4^- and the TiO_2 is an indication of the formation of surface sulfate groups, as reported in previous

studies [10,12,23,54]. This strong interaction between the HSO_4^- and the TiO_2 further confirms the stated higher thermal stability compared to the WO_3 or V_2O_5 based systems.

Based on the calculated geometries, for all systems, the vibrational spectra were calculated for both the share of the NH_4^+ and the HSO_4^- (Figure 10). All calculated spectra are in good agreement with the experimental data with respect to the expected absorption bands. This means, for the spectra calculated for the NH_4HSO_4 all bands predicted by DFT calculation can be assigned to the bands found in the experimental spectra, even though the band intensities are somewhat overestimated for the NH_4^+ species. The same holds true for NH_4HSO_4/WO_3, NH_4HSO_4/V_2O_5 and NH_4HSO_4/TiO_2. From this, we conclude that the geometries obtained from the calculations are representative for the geometries of the sulfates formed on the oxides discussed above. This further strengthens the conclusion that NH_4HSO_4 is a good model substance for the sulfur-containing deposits formed on VWT-type catalysts under SCR conditions in the presence of SO_2.

Furthermore, the differences in thermal stability of NH_4HSO_4 on the investigated oxidic materials is mainly governed by the hydrogen bonding interactions between the HSO_4^- and the metal oxide, whereby a higher degree in stabilizing interactions leads to an increase in thermal stability. However, some HSO_4^--related bands in the calculated spectra exhibit a significant blue shift compared to the experimental data. This is most evident for the TiO_2-based system (Figure 10(b)). This blue shift could be an indication of an overestimation of the strong interaction between the O-atom of the HSO_4^- and the metal oxide by the formation of surface sulfate groups. As stated in the literature [12,54], this surface sulfate groups form at temperatures above 653 K, whereas the DRIFTS experiments were performed at 423 K. Therefore, neither the sample preparation nor the conditions during DRIFTS experiments can account for the surface sulfate formation.

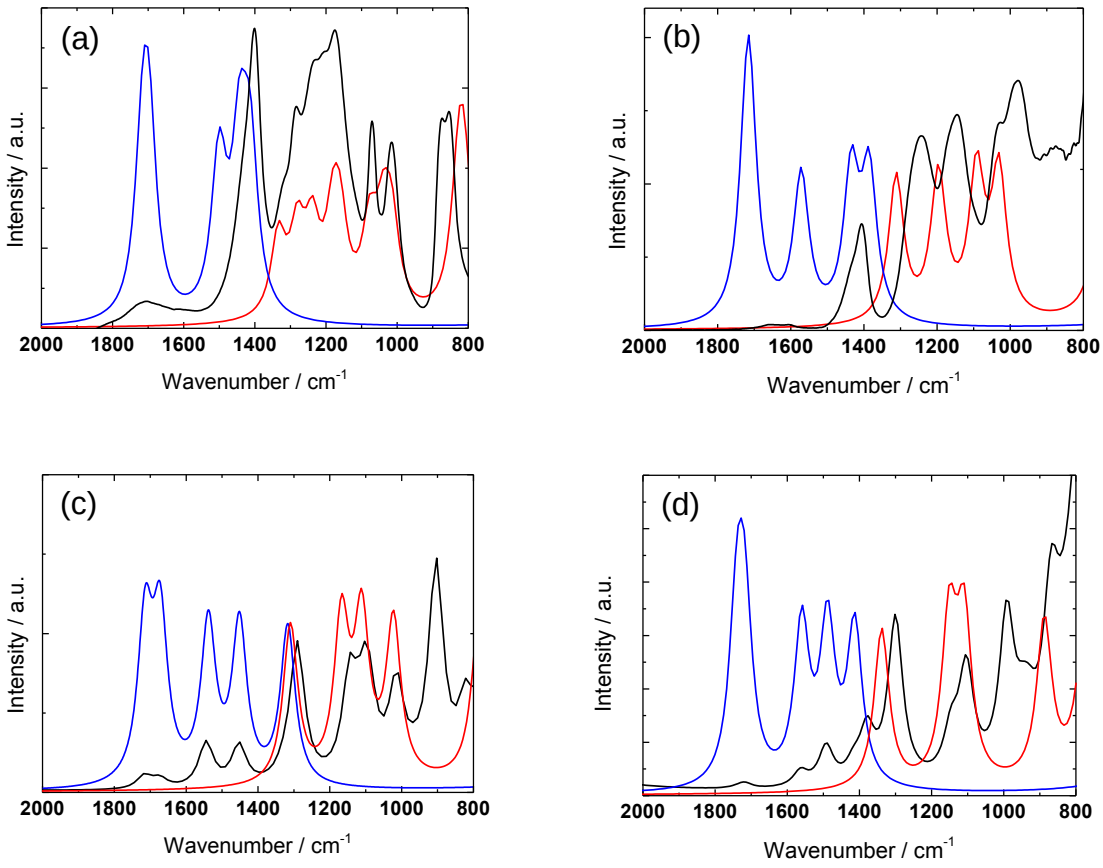

Fig. 10: DRIFTS experiments and calculated vibrational spectra from DFT for (a)(a) NH_4HSO_4, (b) NH_4HSO_4/TiO_2, (c) NH_4HSO_4/V_2O_5, (d) NH_4HSO_4/WO_3 (experimental data – black, calculated share of NH_4^+ - blue, calculated share of HSO_4^- - red)

To further support the agreement between DFT calculations and our experimental data, the concept of substrate support interaction based on electronegativities was used. According to various works available in the literature, the electronegativity of the metal atom in the metal oxide governs the reactivity of the supported species [55]. However, up to date, this was mainly investigated with respect to the activity of supported catalytically active materials, i.e., V_2O_5, in different test reactions such as the oxidation of hydrocarbons [56–58]. In this context, the electronegativities of the metal atoms in the used metal oxides were calculated and correlated with the listed values from the Pauling scale. Al_2O_3 was selected as a lower-end reference material. MoO_3 was used as additional reference material filling the gap between V_2O_5 and WO_3. In addition, MoO_3 is also used as a promoter in vanadia-type SCR catalysts and, as such, is of interest in this context [17]. To calculate the electronegativites, Bader analysis was used. Regarding the absolute values, one has to keep in mind that the employed approach was designed for investigating the in-molecule electronegativities in organic molecules [49]. Figure 11 shows the correlation between the calculated

electronegativities of the metal atom in the free metal oxide and the electronegativities listed in the Pauling scale. As can be seen, the qualitative agreement between listed and calculated values is sufficiently good to differentiate between the different metal oxides. However, the calculated electronegativities represent the values within the whole system. As such, the values differ whether or not the metal oxide is loaded with NH_4HSO_4, while the qualitative correlation stays the same. For the loaded metal oxides, the electronegativity values are lower in comparison to the values of the unloaded material (Figure **Error! Reference source not found.**). In addition, the electronegativities of the S-atoms of the NH_4HSO_4 were calculated. As can be seen from Figure **Error! Reference source not found.**, for increasing electronegativity values of the metal atom, the electronegativity decreases for the corresponding S-atom. This points at a direct interaction between the metal oxide and the NH_4HSO_4 in a way that electron density is transferred to the S-atom, thus weakening the S-O-bonds. Such an interaction is consistent with the decreasing decomposition temperature of the NH_4HSO_4 with increasing electronegativity of the corresponding metal atom. A similar effect was already suggested by Qu et al. [30], who state that the transfer of electron density from the metal oxide to the S-atom enhances the reducibility of the S-atom thus decreasing the thermal stability of NH_4HSO_4 loaded on metal oxides.

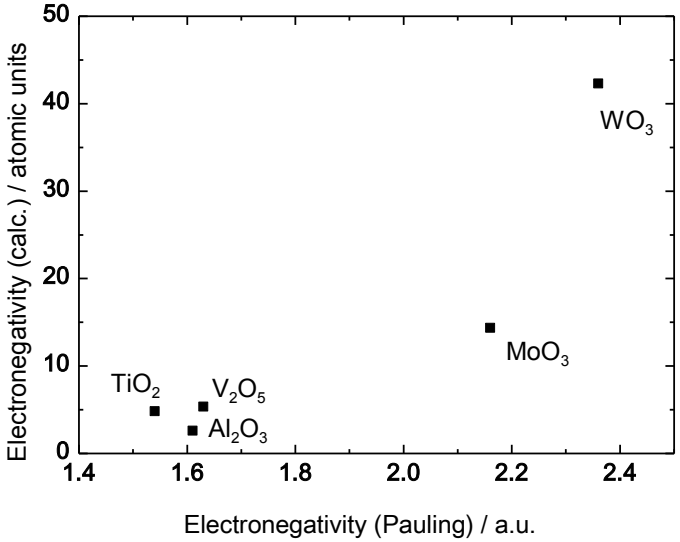

Fig. 11: Listed (Pauling) and calculated electronegativities of the metal atom in the free metal oxide (not loaded with NH_4HSO_4).

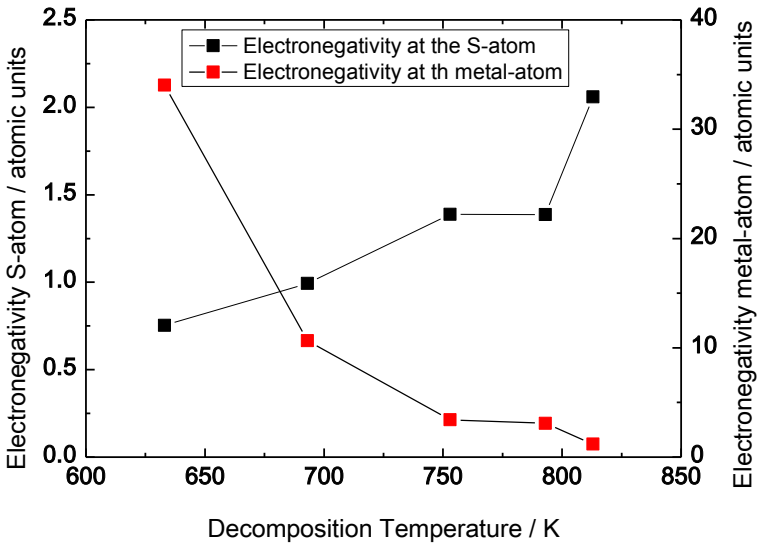

Fig. 12: Electronegativity of the metal atoms and sulfur atoms for the metal oxides (TiO_2, V_2O_5, Al_2O_3, WO_3, MoO_3) loaded with NH_4HSO_4 as a function of the corresponding decomposition temperature of the NH_4HSO_4 determined by TGA (see Figure 6).

4. Conclusions

The formation of sulfur-containing deposits formed on VWT-type catalysts during SCR-DeNO$_x$ with ammonia at elevated pressure in the presence of SO_2 is strongly enhanced at low reaction temperatures. Higher reaction pressure also leads to increased deposit formation due to higher concentrations of SO_2 and O_2 as well as higher residence time of the gas phase on the catalyst. Using DRIFTS and TGA experiments, the formed sulfur-containing deposits were shown to be mainly NH_4HSO_4 as long as the reaction temperature during SCR is above 523 K. At lower temperature, $(NH_4)_2SO_4$ is formed. At higher temperatures, $(NH_4)_2SO_4$ reacts with NO from the gas phase under NH_3 release forming NH_4HSO_4. NH_4HSO_4 is, therefore, a suitable model substance to study the interaction of sulfur-containing deposits formed on oxidic SCR-DeNO$_x$ catalysts at typical application temperatures and pressures.

The thermal stability of NH_4HSO_4 strongly depends on the type of metal oxide used as support and strongly varies from 620 to 820 K. As supported by DFT calculations using Bader analysis, the stability of supported NH_4HSO_4 is predominantly governed by hydrogen bonding of the hydrogen sulfate anions with the metal oxide surface. Increasing electronegativity of the metal atoms in the support oxide weakens the S-O bonds of the hydrogen sulfates leading to lower NH_4HSO_4 decomposition temperatures. These insights can directly be applied to design catalysts with enhanced stability towards as well as facilitated removal of sulfur-containing deposits.

Conflict of interest statement

On behalf of all authors, the corresponding author states that there is no conflict of interest.

References

[1] Y. Hu, K. Griffiths, P.R. Norton, Surface Science 603 (2009) 1740-1750.

[2] M. Selvam, M. Vigneshwaran, R. Irudhayaraj, S. Palani, Indian Journal of Science and Technology 9 (2016).

[3] C. Brüstle, M. Downey, M. Subramaniam, A. Birckett, D. Tomazic (Ed.), Aftertreatment in a Pre-Turbo Position: Size and Fuel Consumption Advantage for Tier 4 Large-Bore Diesel Engines, 2011.

[4] O. Kröcher, M. Elsener, M.-R. Bothien, W. Dölling, MTZ (2014) 68-73.

[5] V. Joergl, P. Keller, O. Weber, K. Mueller-Haas, R. Konieczny, SAE Technical paper.

[6] T. Fujibayashi, S. Baba, H. Tanaka, CIMAC Congress 2013, Shanghai (2013).

[7] T. Rammelt, B. Torkashvand, C. Hauck, J. Böhm, R. Gläser, O. Deutschmann, Emiss. Control Sci. Technol. 3 (2017) 275-288.

[8] R. Bank, B. Buchholz, H. Harndorf, R. Rabe, U. Etzien, Analyse des Konversionsverhaltens von SCR-Katalysatoren unter den Betriebsbedingungen IMO Tier III konformer Großdieselmotoren, 2. Rostocker Großmotorentagung, Rostock, 17.09.2012.

[9] J.P. Dunn, J.-M. Jehng, S. Du Kim, L.E. Briand, H.G. Stenger, I.E. Wachs, J. Phys. Chem. B 102 (1998) 6212-6218.

[10] J. Svachula, L.J. Alemany, N. Ferlazzo, P. Forzatti, E. Tronconi, F. Bregani, Ind. Eng. Chem. Res. 32 (1993) 826-834.

[11] H. Kamata, H. Ohara, K. Takahashi, A. Yukimura, Y. Seo, Catal. Lett. 73 (2001) 79-83.

[12] J.P. Chen, M.A. Buzanowski, R.T. Yang, J.E. Cichanowicz, J. Air Waste Manage. Assoc. 40 (1990) 1403-1409.

[13] J.P. Dunn, P.R. Koppula, H. G. Stenger, I.E. Wachs, Appl. Catal. B 19 (1998) 103-117.

[14] L. Zhang, L. Li, Y. Cao, X. Yao, C. Ge, F. Gao, Y. Deng, C. Tang, L. Dong, Appl. Catal. B 165 (2015) 589-598.

[15] M. Magnusson, E. Fridell, H.H. Ingelsten, Appl. Catal. B 111-112 (2012) 20-26.

[16] G. Baltin, H. Köser, K.-P. Wendlandt, Catal. Today 75 (2002) 339-345.

[17] L. Song, J. Chao, Y. Fang, H. He, J. Li, W. Qiu, G. Zhang, Chem. Eng. J. 303 (2016) 275-281.

[18] Z. Huang, J. Catal. 214 (2003) 213-219.

[19] Z. Huang, Z. Zhu, Z. Liu, Appl. Catal. B 39 (2002) 361-368.

[20] W. Xu, H. He, Y. Yu, J. Phys. Chem. C 113 (2009) 4426-4432.

[21] S. Zang, G. Zhang, W. Qiu, L. Song, R. Zhang, H. He, Chinese J. Catal. 37 (2016) 888-897.

[22] C. Li, M. Shen, T. Yu, j. wang, J. Wang, Y. Zhai, Phys. Chem. Chem. Phys. (2017).

[23] R. Khodayari, C.U. Ingemar Odenbrand, Appl. Catal. B 33 (2001) 277-291.

[24] H.H. Phil, M.P. Reddy, P.A. Kumar, L.K. Ju, J.S. Hyo, Appl. Catal. B 78 (2008) 301-308.

[25] S. Matsuda, T. Kamo, A. Kato, F. Nakajima, T. Kumura, H. Kuroda, Ind. Eng. Chem. Prod. Res. Dev. 21 (1982) 48-52.

[26] P. Ji, X. Gao, X. Du, C. Zheng, Z. Luo, K. Cen, Catal. Sci. Technol. 6 (2016) 1187-1194.

[27] B. Shen, F. Wang, B. Zhao, Y. Li, Y. Wang, J. Ind. Eng. Chem. 33 (2016) 262-269.

[28] Y.-J. Shi, H. SHU, Y.-h. ZHANG, H.-M. Fan, Y.-P. Zhang, L.-j. YANG, Fuel Processing Technology (2016).

[29] D. Ye, R. Qu, H. Song, X. Gao, Z. Luo, M. Ni, K. Cen, Chem. Eng. J. 283 (2016) 846-854.

[30] D. Ye, R. Qu, H. Song, C. Zheng, X. Gao, Z. Luo, M. Ni, K. Cen, RSC Adv. 6 (2016) 55584-55592.

[31] Q. Li, S. Chen, Z. Liu, Q. Liu, Appl. Catal. B 164 (2015) 475-482.

[32] Z. Ma, X. Wu, Y. Feng, Z. Si, D. Weng, L. Shi, Progress in Natural Science: Materials International 25 (2015) 342-352.

[33] Z. Zhu, H. Niu, Z. Liu, S. Liu, J. Catal. 195 (2000) 268-278.

[34] P. Li, Q. Liu, Z. Liu, Chem. Eng. J. 181-182 (2012) 169-173.

[35] I.K. Thege, Thermochimica Acta 60 (1983) 149-159.

[36] D.A. Kosova, A.L. Emelina, M.A. Bykov, Thermochimica Acta 595 (2014) 61-66.

[37] W. Yang, F. Liu, L. Xie, Z. Lian, H. He, Ind. Eng. Chem. Res. 55 (2016) 2677-2685.

[38] Z. Zhu, Z. Liu, H. Niu, S. Liu, T. Hu, T. Liu, Y. Xie, J. Catal. 197 (2001) 6-16.

[39] J. Li, Y. Peng, H. Chang, X. Li, J.C. Rittenden, J. Hao, Front. Environ. Sci. Eng. (2016).

[40] S. Bai, Z. Wang, H. Li, X. Xu, M. Liu, Fuel 194 (2017) 36-41.

[41] L. Wei, S. Cui, H. Guo, X. Ma, L. Zhang, J. Mol. Catal. A: Chem. 421 (2016) 102-108.

[42] Q. Wu, H. Gao, H. He, J. Phys. Chem. B 110 (2006) 8320-8324.

[43] X. Du, X. Gao, K. Qiu, Z. Luo, K. Cen, J. Phys. Chem. C 119 (2015) 1905-1912.

[44] E. Broclawik, A. Góra, M. Najbar, J. Mol. Catal. A: Chem. 166 (2001) 31-38.

[45] G. te Velde, F.M. Bickelhaupt, E.J. Baerends, C. Fonseca Guerra, van Gisbergen, S. J. A., J.G. Snijders, T. Ziegler, J. Comput. Chem. 22 (2001) 931-967.

[46] C. Fonseca Guerra, J.G. Snijders, G. te Velde, E.J. Baerends, Theoretical Chemistry Accounts: Theory, Computation, and Modeling (Theoretica Chimica Acta) 99 (1998) 391-403.

[47] E.J. Baerends, T. Ziegler, A.J. Atkins, J. Autschbach, et al., ADF2017, SCM, Theoretical Chemistry, Vrije Universiteit, Amsterdam, The Netherlands, https://www.scm.com.

[48] X. Du, X. Gao, W. Hu, J. Yu, Z. Luo, K. Cen, J. Phys. Chem. C 118 (2014) 13617-13622.

[49] V. Tognetti, C. Morell, L. Joubert, Chem. Phys. Lett. 635 (2015) 111-115.

[50] P.W. Seo, K.H. Park, S.C. Hong, J. Ind. Eng. Chem. 16 (2010) 283-287.

[51] National Institute of Advanced Industrial Science and Technology, SDBS, available at http://sdbs.db.aist.go.jp (accessed on 12.03.2017).

[52] P. Li, Z. Liu, Q. Li, W. Wu, Q. Liu, Ind. Eng. Chem. Res. 53 (2014) 7910-7916.

[53] X. Guo, C. Bartholomew, W. Hecker, L.L. Baxter, Appl. Catal. B 92 (2009) 30-40.

[54] X.H. Lin, X.J. Yin, J.Y. Liu, S.F. Yau Li, Appl. Catal. B 203 (2017) 731-739.

[55] G. Tsilomelekis, A. Christodoulakis, S. Boghosian, Catal. Today 127 (2007) 139-147.

[56] I.E. Wachs, Catalysis 13 (1997) 37-54.

[57] I.E. Wachs, Catal. Today 100 (2005) 79-94.

[58] A. Dinse, B. Frank, C. Hess, D. Habel, R. Schomäcker, J. Mol. Catal. A: Chem. 289 (2008) 28-37.